Accepted Manuscript

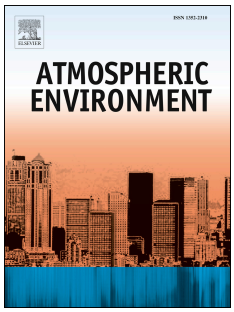

Warming effect of dust aerosols modulated by overlapping clouds below

Hui Xu, Jianping Guo, Yuan Wang, Chuanfeng Zhao, Zhibo Zhang, Min Min, Yucong Miao, Huan Liu, Jing He, Shunwu Zhou, Panmao Zhai

PII: S1352-2310(17)30477-6

DOI: 10.1016/j.atmosenv.2017.07.036

Reference: AEA 15450

To appear in: *Atmospheric Environment*

Received Date: 14 March 2017

Revised Date: 18 July 2017

Accepted Date: 19 July 2017

Please cite this article as: Xu, H., Guo, J., Wang, Y., Zhao, C., Zhang, Z., Min, M., Miao, Y., Liu, H., He, J., Zhou, S., Zhai, P., Warming effect of dust aerosols modulated by overlapping clouds below, *Atmospheric Environment* (2017), doi: 10.1016/j.atmosenv.2017.07.036.

Warming effect of dust aerosols modulated by overlapping clouds below

Hui Xu[1], Jianping Guo[1]*, Yuan Wang[2], Chuanfeng Zhao[3], Zhibo Zhang[4], Min Min[5], Yucong Miao[1], Huan Liu[1], Jing He[1], Shunwu Zhou[6], Panmao Zhai[1]

[1]State Key Laboratory of Severe Weather, Chinese Academy of Meteorological Sciences, Beijing 100081, China.

[2]Division of Geological and Planetary Sciences, California Institute of Technology, Pasadena, CA 91125, USA.

[3]College of Global Change and Earth System Science, Beijing Normal University, Beijing 100875, China.

[4]Physics Department/JCET, University of Maryland, Baltimore County, MD 21250, USA.

[5]National Satellite Meteorological Center, Chinese Meteorological Administration, Beijing 100081, China.

[6]College of Atmospheric Science, Nanjing University of Information Sciences & Technology (NUIST), Nanjing 210044, China.

Correspondence to:

Dr. Jianping Guo (jpguocams@gmail.com)

Abstract

Due to the substantial warming effect of dust aerosols overlying clouds and its poor representation in climate models, it is imperative to accurately quantify the direct radiative forcing (DRF) of above-cloud dust aerosols. When absorbing aerosol layers are located above clouds, the warming effect of aerosols strongly depends on the cloud macro- and micro-physical properties underneath, such as cloud optical depth and cloud fraction at visible wavelength. A larger aerosol-cloud overlap is believed to cause a larger warming effect of absorbing aerosols, but the influence of overlapping cloud fraction and cloud optical depth remains to be explored. In this study, the impact of overlapping cloud properties on the shortwave all-sky DRF due to springtime above-cloud dust aerosols is quantified over northern Pacific Ocean based on 10-year satellite measurements. On average, the DRF is roughly 0.62 Wm^{-2}. Furthermore, the warming effect of dust aerosols linearly increases with both overlapping cloud fraction and cloud optical depth. An increase of 1% in overlapping cloud fraction will amplify this warming effect by 1.11 $Wm^{-2}\tau^{-1}$. For the springtime northern Pacific Ocean, top-of-atmosphere cooling by dust aerosols turns into warming when overlapping cloud fraction is beyond 0.20. The variation of critical cloud optical depth beyond which dust aerosols switch from exerting a net cooling to a net warming effect depends on the concurrent overlapping cloud fraction. When overlapping cloud coverage range increases from 0.2-0.4 to 0.6-0.8, the corresponding critical cloud optical depth reduces from 6.92 to 1.16. Our results demonstrate the importance of overlapping cloud properties for determining the springtime warming effect of dust aerosols.

1 Introduction

Dust aerosols play an important role on regional and global energy budget directly by scattering and absorbing the shortwave solar radiation, while the magnitude remains uncertain (Sokolik et al., 2001; IPCC, 2007; Wang et al., 2010). The direct radiative forcing (DRF) of dust aerosols at top-of-atmosphere (TOA) is strongly dependent on both the albedo of the underlying surface and the optical and microphysical properties of dust aerosols (Shen and Wei, 2000; Wang et al., 2013). Over dark surfaces (e.g. Ocean), the scattering effect of dust aerosols in clear-sky is generally predominant, leading to a negative DRF (i.e., cooling) at TOA. However, when dust aerosols reside above cloud, the absorption of dust aerosol particles on solar radiation can be significantly enhanced by cloud reflection, which can offset or even mask the scattering effect of the aerosol. Thus, above-cloud dust aerosols (ACDA) produce a lessoned negative effect or even positive effect at TOA (Abel et al., 2005; Chand et al., 2009; Keil and Haywood, 2003; Meyer et al., 2013; Zhang et al., 2014), and thus potentially affect the regional radiation budget, hydrological cycle and large-scale circulations (Wang et al., 2014; Wang et al., 2015; Guo et al., 2016a; Li et al., 2016; Guo et al., 2017a). During springtime, dust aerosols from arid and semi-arid regions of China and Mongolia can travels a long distance off the eastern coasts of China and sometimes reaches North America beyond the Pacific Ocean (Holzer et al. 2003; Dai et al., 2015). Due to the high cloud fraction over the Pacific Ocean throughout the year, there are frequent occurrences of dust aerosols residing above low-level clouds over this region (Murayama et al., 2001; Zhang et al., 2016). Thus, an accurate quantification of TOA DRF of springtime ACDA over northern Pacific Ocean is necessary to improve the assessment of their climate impacts.

It is well known that the estimation of the TOA DRF of aerosols overlying clouds depends largely on the single scattering albedo (ω) of aerosols (Chand et al., 2009). As ω is less than 0.83, aerosols tend to lead to a warming effect at the top-of-atmosphere. In contrast, aerosols tend to lead to a cooling effect as ω exceeds 0.91 (at visible wavelengths) (Podgorny and Ramanathan, 2001). Noh (2014) comprehensively documented the vertically-resolved and total layer-mean ω of the mixed-dust plumes using multiwavelength Raman lidar, and found that the ω value (532 nm) of Asian dust plumes mixed with industrial/urban pollution particles range 0.71 to 0.95.

However, the impact of the uncertainty of ω on the estimation of the warming effect of dust aerosols overlying clouds remains unknown.

To represent the global and regional DRF of above-cloud aerosols accurately, the large-scale measurements of aerosol and cloud properties, and aerosol-cloud overlap are needed (de Graaf et al., 2014; Devasthale and Thomas, 2011), which can only be obtained by satellite. However, passive satellite sensors only provide aerosol retrievals under cloud-free conditions (Kahn et al., 2005; Remer et al., 2005). Until recently, A-Train, a constellation of several satellites carrying a suite of active and passive sensors with enhanced capabilities emerged (Stephens et al., 2002), has been able to provide global-scale measurements of above-cloud aerosols. Active sensors such as the Cloud-Aerosol Lidar with Orthogonal Polarization (CALIOP) onboard the Cloud-Aerosol Lidar and Infrared Pathfinder Satellite Observation (CALIPSO) satellite can measure the properties of aerosols even on a cloudy day, as long as the aerosol layer is situated above the clouds (Winker et al., 2009; Guo et al., 2016b). Combining the CALIOP data with measurements of regional cloud cover from the Moderate Resolution Imaging Spectroradiometer (MODIS), Chand et al. (2009) showed that the regional mean DRF of aerosols is strongly dependent on underlying cloud fraction (CF). A larger CF will cause a larger warming effect of aerosols. They also defined the critical CF at which the TOA DRF of above-cloud aerosols changes sign from negative to positive. On global scale, the shortwave DRF due to above-cloud aerosols are also found modulated by the optical depth of cloud (COD) (Zhang et al., 2014). Apart from the underlying CF and COD, whether aerosols exert a net positive or negative direct radiative forcing, is shown to be influenced by spatial distribution of cloud with respect to the overlying aerosol layers (Chand et al., 2009). As the amount of overlap increases, the system is likely to exert a net warming effect in case of absorbing aerosols (Devasthale and Thomas, 2011, 2011). However, few efforts have been devoted to quantitatively explore how overlapping COD and CF impact the DRF of above–cloud aerosols.

The objective of the present study is to assess the impact of overlapping CF and COD clouds on the springtime warming effect of dust aerosols. As such, we estimate 10-years (2007-2016) shortwave all-sky TOA DRF due to springtime ACDA over the northern Pacific Ocean based on long-term CALIOP data and simultaneous MODIS observations.

2 Study area

During the spring season, the major sources of dust aerosols are the Taklimakan Desert in western China and the Gobi desert in Mongolia and northern China (Zhang et al., 1993; Sun et al., 2001). Dust aerosols lifted by the strong surface level westerly winds can travels a long distance off the eastern coasts of China to Japan (Ma et al., 2005), Korea (Mori et al., 2003; Kim et al., 2004), and even further to North America beyond the Pacific Ocean (Huang et al., 2010). During the same time period, large amounts of low level clouds are also present over northern Pacific Ocean (Devasthale and Thomas, 2011), resulting in high occurrence frequency of ACDA over this region (~10%) (Zhang et al., 2016). Figure 1 shows an example of dust aerosol features resided over cloud features during a daytime CALIPSO pass on 1st April 2007. Over Ocean, the RGB composite image of MODIS data shows the clouds in white and the dust aerosols in yellow. When dark yellow dust passes over the bright white cloud deck, it reduces the clouds' ability to reflect solar radiation sunlight back to space and darkens the scenes. As also illustrated in Figure 1, the dust aerosol particles are widely observed over the northeastern part of China, Korea and Japan, which further corroborated that the aerosols above clouds is dust aerosols. In this study, the northern Pacific Ocean within the region (20°N-60°N, 110°E-110°W) is chosen in attempt to analyze the impact of overlapping cloud properties on the springtime warming effect of dust aerosols. The time period refers to the springtime (March–May) for the period from 2007 to 2016.

3 Data

3.1 CALIOP aerosol and cloud layer products

The space-borne lidar CALIOP, on board the CALIPSO satellite, was launched in April 2006 (Winker et al., 2007). CALIOP are in a 705 km sun-synchronous polar orbit with an equator-crossing time of about 1:30 PM, local solar time. The orbit is controlled to repeat the same ground track every 16 days with cross-track errors of less than ±10 km. The orbit inclination of 98.2° provides global coverage between 82°N and 82°S. Using the two 532-nm receiver channels and a channel measuring the total 1064-nm return signal, CALIOP measures the detailed vertical distribution of aerosols and clouds along with their microphysical and optical properties (Winker et al., 2009). The CALIOP level 1B data products reports the profiles of attenuated backscatter

coefficients (Powell et al. 2009). Based on these level 1 profiles, aerosol and cloud layers are detected using "feature finder" algorithm and cloud-aerosol discrimination (CAD) algorithm. And their top and bottom heights and layer integrated properties are record in CALIOP level 2 products (Vaughan et al. 2004; Vaughan et al., 2009).

In this study, we use CALIOP level-2 Version 3 aerosol and cloud layer products of "CAL_LID_L2_05kmALay" and "CAL_LID_L2_05kmCLay" at a nominal 5 km horizontal resolution for above-cloud aerosol pixels identification, and for information on the properties of aerosol layers, including aerosol type, AOD, and layer top and bottom height. The detected aerosol layers are further classified into six sub-types, including polluted continental, biomass burning, desert dust, polluted dust, clean continental and marine (Omar et al., 2009). We only consider the dust aerosols in this paper. In addition to physical properties, the CALIOP layer products also provide various metrics and flags on data quality assurance. These include cloud-aerosol discrimination (CAD) score (Liu et al., 2009), horizontal averaging scale, extinction quality control (QC) flag, and estimated uncertainty of the layer AOD. Here, we apply these metrics (see Table 1) suggested by the CALIPSO science team to screen for reliable retrievals (e.g., Winker et al., 2013). Prior to the calculation of DRF, all of the valid AOD data along the ground track of CALIOP are averaged over a 1º×1º grid.

3.2 MODIS daily level-3 cloud property product

The MODIS instrument is aboard the Earth Observing System (EOS) Terra and Aqua satellites, launched in 1999 and 2002, respectively. MODIS scans a swath width of 2330 km that is sufficiently wide to provide nearly complete global coverage every two days from a polar-orbiting, sun-synchronous, platform at an altitude of 705 km (Salomonson et al., 1989; Remer et al., 2005). MODIS measures the TOA radiance with 36 spectral bands from 0.415 to 14.235 μm with spatial resolutions of 250 m (two bands), 500 m (five bands), and 1000 m (29 bands). Twenty-six bands are used to derive cloud physical and optical properties such as cloud optical thickness, cloud effective particle radius, cloud water path, as well as cloud fraction (Platnick et al., 2003).

MODIS Level-3 MOD08 (Terra) and MYD08 (Aqua) datasets are summarized over a 1°×1° global grid for daily time scales (Levy et al., 2009). In this paper, we use the collection 051

MYD08 dataset for information on the physical and radiative properties of clouds collocated with dust aerosols atop, including the daily averaged COD at 860 nm, cloud phase, cloud effective radius and cloud fraction.

3.3 Ancillary Aerosol Index information

The Ozone Monitoring Instrument (OMI) is flown on NASA's EOS Aura spacecraft in July 15, 2004. The Aura spacecraft circulates in a 98.2° inclination, sun-synchronous polar orbit at 705-km altitude, with a local afternoon equator crossing time at 13:45 (ascending node), providing 14 orbits a day. OMI measures the complete spectrum in the ultraviolet–visible (UV/VIS) wavelength range with a very high spatial resolution (13 km×24 km) and daily global coverage (Levelt et al., 2006). As is well known that there exist large uncertainties of MODIS AOD in spring over northeastern Asian countries due to the high terrestrial surface reflectivity, we have to use the Aerosol Index (AI) product derived from OMI. The AI is retrieved based on two UV channels, which shows high accuracy in charactering dust aerosol loading in spring (Herman et al., 1997; Torres et al., 2007). Therefore, AI dataset here has been utilized to investigate the spatial pattern of springtime dust aerosols and their trans-Pacific transport from arid and semi-arid regions of China and Mongolia to North America (Guo et al., 2017b).

3.4 Radiative transfer model RRTM_SW

The calculation of the shortwave DRF of above-cloud dust aerosols requires an appropriate radiative transfer model. As such, here we use the RRTM_SW (shortwave rapid radiative transfer model), from which fluxes and heating rates can be derived for the shortwave spectral regime (from 820 to 50,000 cm-1). The model outputs can be generally applied to the studies associated with atmospheric radiative transfer and general circulation models (GCMs) (Clough et al., 2005).

4 Methods

First of all, occurrence frequency of ACDA is calculated for each 1° × 1° grid containing ACDA pixels based on the CALIOP aerosol and cloud profiling data (Section 4.1). Second, their corresponding TOA shortwave all-sky DRFs will be quantified, using the CALIOP and MODIS

observations, in combination with the RRTM_SW model simulations over northern Pacific Ocean (Section 4.2).

4.1 Computation of occurrence frequency of above-cloud dust aerosols

For each 1°×1° grid box, the ACDA occurrence frequency (f_{ACDA}) is defined as the ratio of ACDA columns to total cloudy columns sampled by CALIOP, following Zhang et al. (2016):

$$f_{ACDA}(t^*) = \frac{N_{ACDA}}{N_{cloudy}} \quad (1)$$

where t^* denotes the CALIOP crossing time, f_{ACDA} denotes the fraction of cloudy columns with dust aerosols overlying clouds, N_{cloudy} is the total number of cloudy columns sampled by CALIOP within the grid, and N_{ACDA} is the number of ACDA columns that have been identified as the dust aerosol by CALIOP.

4.2 Computation of all-sky TOA DRF due to ACDA

4.2.1 Definitions of the all-sky TOA DRF due to ACDA

For each 1°×1° grid box, diurnal average shortwave all-sky TOA DRF ($\overline{\Delta F_{all-sky}}$ in units of Wm^{-2}) containing ACDA is calculated following Min and Zhang (2014):

$$\overline{\Delta F_{all-sky}} = \frac{1}{24}\int_{T_{sunrise}}^{t_{sunset}} \{[1 - f_c(t)]\Delta F_{clear-sky}[\theta^0(t), \tau_a(t)] + f_c(t)\Delta F_{cloudy-sky}[\theta^0(t), \tau_a(t), \tau_c(t)]\}dt \quad (2)$$

where the upper bar "-" indicates the diurnal average, the normalization factor 1/24 is to obtain the diurnal average from hourly instantaneous computations, $f_c(t)$ denotes the instantaneous cloud fraction, $\Delta F_{clear-sky}(t)$ and $\Delta F_{clear-sky}(t)$ represent the hourly instantaneous DRF over the clear-sky and cloudy-sky region of the grid, respectively, $\theta^0(t)$ is the instantaneous solar zenith angle, $\tau_a(t)$ and $\tau_c(t)$ stands for the instantaneous AOD and COD, respectively. Because the orbit of CALIOP only provides a single snapshot of the diurnal cycle during daytime (another during night time), we omit the diurnal variation of τ_a, and only use the value during the

daytime CALIOP at time t* (roughly 1:30 p.m. local time). As such, we can rewrite the $\overline{\Delta F_{all-sky}}$ as follows:

$$\overline{\Delta F_{all-sky}} \approx [1 - f_c(t^*)] \times \frac{1}{24}\int_{T_{sunrise}}^{t_{sunset}} \Delta F_{clear-sky}[\theta^0(\mathrm{t}), \tau_a(t^*)]dt + f_c(t^*) \times \frac{1}{24}\int_{T_{sunrise}}^{t_{sunset}} \Delta F_{\mathrm{cloudy}-sky}[\theta^0(\mathrm{t}), \tau_a(t^*), \tau_c(t^*)]dt \quad (3)$$

In Eq. (3), cloudy-sky DRF of dust aerosols includes the DRF of dust aerosols above-cloud, below-cloud and within cloud. Here we simply assume cloudy-sky aerosol DRF mainly contributed to ACDAs. This is a reasonable assumption for TOA DRF (Zhang et al., 2016). Based on this assumption, we can rewrite Eq. (3) as:

$$\overline{\Delta F_{all-sky}} \approx [1 - f_c(t^*)] \times \frac{1}{24}\int_{T_{sunrise}}^{t_{sunset}} \Delta F_{clear-sky}[\theta^0(\mathrm{t}), \tau_a(t^*)]dt + f_c(t^*) \times f_{ACDA}(t^*) \frac{1}{24}\int_{T_{sunrise}}^{t_{sunset}} \Delta F_{ACDA}[\theta^0(\mathrm{t}), \tau_a(t^*), \tau_c(t^*)]dt \quad (4)$$

where $f_{ACDA}(t^*)$ is the occurrence frequency of ACDA observed at the CALIOP crossing time defined in Eq. (1), and $\Delta F_{ACDA}(t^*)$ is the hourly instantaneous DRF of ACDA.

4.2.2 Computation of instantaneous all-sky TOA DRF due to ACDA

As shown in Eq. (4), once the instantaneous $\Delta F_{ACDA}(t^*)$ and $\Delta F_{clear-sky}(t^*)$ is known, we can easily obtain $\overline{\Delta F_{all-sky}}$ from the integral. In this section, we explain how the instantaneous $\Delta F_{ACDA}(t^*)$ and $\Delta F_{clear-sky}(t^*)$ are computed. Generally speaking, the ΔF_{ACDA} is defined as the difference between the net flux with aerosol above cloud and that without aerosol above cloud, which can be expressed as:

$$\Delta F_{ACDA} = F_{net,ACDA} - F'_{net,ACDA} \quad (5)$$

where $F_{net,ACDA}$ represents the net flux with aerosol above cloud, and $F'_{net,ACDA}$ represents the net flux without aerosol above cloud.

$F_{net,ACDA}$ can be calculated as the difference between the downwelling flux with aerosol above cloud ($F_{\downarrow,ACDA}$) and upwelling flux with aerosol above cloud ($F_{\uparrow,ACDA}$), as given as below:

$$F_{net,ACDA} = F_{\downarrow,ACDA} - F_{\uparrow,ACDA} \quad (6)$$

Similarly, $F'_{net,ACDA}$ denotes the difference between the downwelling flux without aerosol above cloud ($F'_{\downarrow,ACDA}$) and the upwelling flux without aerosol above cloud ($F'_{\uparrow,ACDA}$), which is formulated as:

$$F'_{net,ACDA} = F'_{\downarrow,ACDA} - F'_{\uparrow,ACDA} \quad (7)$$

Combining Eq. (5-7), we obtain the following expression:

$$\Delta F_{ACDA} = (F_{\downarrow,ACDA} - F_{\uparrow,ACDA}) - (F'_{\downarrow,ACDA} - F'_{\uparrow,ACDA}) \quad (8)$$

Since the downward flux at the top-of-atmosphere is independent of the presence of aerosols above cloud (i.e., $F_{\downarrow,ACDA}$=$F'_{\downarrow,ACDA}$), we can rewrite Eq. (8) as:

$$\Delta F_{ACDA} = F'_{\uparrow,ACDA} - F_{\uparrow,ACDA} \quad (9)$$

Similar to ΔF_{ACDA}, the $\Delta F_{clear-sky}$ is formulated as:

$$\Delta F_{clear-sky} = F'_{\uparrow,clear-sky} - F_{\uparrow,clear-sky} \quad (10)$$

where $F'_{\uparrow,clear-sky}$ and $F_{\uparrow,clear-sky}$represent the upwelling flux with and without aerosol in clear sky, respectively.

4.2.3 Radiative transfer simulations

For the simulations of upward flux reaching the top-of-atmosphere over the region where dust aerosols overlie clouds ($F'_{\uparrow,ACDA}$ and $F_{\uparrow,ACDA}$), we derive the AOD (τ_a) from the CALIOP level-2 aerosol layer product and COD (τ_c) and cloud effective radius from MODIS daily level-3 product, all of which serve as key input parameters of the RRTM_SW model. In addition to AOD and COD, the scattering properties of dust aerosols including single scattering albedo (ω) and phase function (g) are also necessary for these simulations. However, the MODIS and CALIOP products could not provide the ω and g. Therefore, here we use ω and g as described in Omar et al. (2009) for dust aerosols in order to be consistent with the CALIOP operational retrieval algorithm. Figure 2 shows the spectrally dependent single scattering albedo and phase function of dust aerosols calculated using Mie code (Wiscombe, 1980) for the RRTM-SW bands. It should be noted that a bimodal lognormal size distribution and a single refractive index of 1.414+0.004i are assumed for all wavelengths (Omar et al., 2009). In order to obtain the simulations of upward flux reaching the top-of-atmosphere over the clear-sky region ($F'_{\uparrow,clear-sky}$

and $F_{\uparrow,\mathrm{clear-sky}}$), only the τ_a, ω and g of dust aerosols have been taken for RRTM_SW model. In addition, a U.S. standard atmosphere model is chosen to set atmospheric vertical profiles of pressure and temperature.

Estimation of DRF strongly depends on the single scattering albedo of aerosols, so sensitivity study is performed by running RRTM_SW for different single scattering albedo values ($0.8 \leq \omega \leq 0.98$) to get the diurnal average all-sky DRF due to above-cloud dust aerosols.

5 Results and discussions

5.1 Occurrence frequency of ACDA

The springtime spatial distribution of ACDA occurrence frequency (OF) over the northern Pacific Ocean is examined in Figure 3a. The maximum OF is observed off the coastal areas of East Asia with values as high as 12%, exhibiting a pronounced decreasing pattern along west-east direction. The spatial distributions of satellite-derived aerosol index (AI) over the dust source region indicate that dust aerosols can be seen across the whole nothern China in spring. Overall, the episodes of ACDA frequent the northern Pacific Ocean due to the high OF detected over there, which is consistent with Devasthale and Thomas (2011). However, much higher OF of 0.1 was revealed by Zhang et al. (2016), which was limited to northwestern Pacific Ocean.

The OF vertical profiles of overlapping dust aerosols and clouds during springtime over the northern Pacific Ocean are shown in Figure 3b. It indicates that the bases of dust aerosols layers are 2-3 km high in most cases while the bulk of cloud layers have their tops within 0.5-1.5 km. Note that the climatological vertical profiles in Figure 3b are averaged over different scenarios during 10 years, so the large overlap between dust and cloud layers near 2 km altitude does not necessarily mean the physical contact between dust particles and clouds. For about 60% of overlapping events, dust aerosol layers are lofted within 1km above underlying cloud layers. In contrast, the cloud layer tops are within 3km below the dust aerosol layer bases for more than 90% of overlapping events (Figure 4).

5.2 Correlational analyses between all-sky TOA DRF due to ACDA and overlapping cloud properties

Since the direct radiative forcing due to aerosols overlying clouds is, apart from the cloud properties beneath the aerosol layers, shown to be influenced by the amount of aerosol-cloud overlap, it is necessary to investigate the impact of the overlapping cloud properties on the direct radiative effect due to above-cloud dust aerosols. To better demonstrate the correlation between the overlapping cloud properties and the direct radiative effect due to above-cloud dust aerosols, here we applied direct radiative forcing efficiency (RFE, defined as the change in DRF per unit AOD change) instead of DRF.

Figure 5a shows the geographical distribution of the correlation coefficients (R) between springtime all-sky TOA RFE due to above-cloud dust aerosols and its occurrence frequency for the period 2007 to 2016. Most of the R value is larger than zero, indicating dust aerosols overlying clouds generally has a warming effect over this region. The reason seems to be that clouds can increase of the absorption of absorbing aerosols of the incident radiation by reflecting a large amount of solar radiation to the atmosphere and above-cloud aerosol layers, leading the above-cloud aerosols has a warming effect on the top-of-atmosphere. As shown in Figure 5b, TOA RFE also has a positive association with underlying cloud fraction, reinforcing further the possible warming effect of dust aerosols.

Similar to the underlying cloud fraction and occurrence frequency of above-cloud dust aerosols, overlapping cloud fraction that only includes the cloud features with overlying aerosol layers is still positively associated with the springtime warming effect of dust aerosols (Figure 5c). This finding is well consistent with previous studies, which demonstrate that both the cloud fractional coverage and its spatial distribution with respect to the overlying aerosol layers exert non-negligible influences on the direct radiative effect of aerosols (Chand et al., 2009). Thus, resolving uncertainties in the estimation of direct radiative effect due to dust aerosols overlying clouds requires sufficient knowledge of how closely dust aerosols and clouds are overlapped (Devasthale and Thomas, 2011).

In addition, the cloud optical depth for the overlapping cloud seems to exhibit ubiquitous positive association with RFE (Figure 5d). Meanwhile, the seasonal mean overlapping cloud

cover and cloud optical depth associated with the below-aerosol clouds over the northern Pacific are as high as 0.74 and 11.35, respectively. It is, therefore, indicative of the potentially large impact of the overlapping cloud fraction and cloud optical depth of below-aerosol cloud layer on the direct radiative effect due to above-cloud dust aerosols.

5.3 Impact of overlapping cloud fraction on all-sky TOA DRF due to ACDA

To further demonstrate the close relationship between the overlapping cloud fraction and springtime warming of dust aerosols, we examine the all-sky TOA RFE due to above-cloud dust aerosols. As inferred from Figure 6, the RFE at TOA for clear-sky conditions is -22.48 W $m^{-2}\tau^{-1}$, whereas the mean value for cloudy sky 88.54 W $m^{-2}\tau^{-1}$. The possible explanation is that, in clear-sky conditions, the presence of dust aerosols over the dark ocean surface enhances the reflection of solar radiation in the Earth system, resulting in a negative forcing. In contrast, the presence of dust aerosols over the bright clouds increases the amount of net TOA radiation by absorbing more radiation in the atmosphere but decreases the amount of solar radiation reflected back to space. In this case, dust aerosols have a positive forcing. And this disparity further reinforces the possibility of the positive radiative effect due to above-cloud dust aerosols. Interestingly, a high linear correlation is found between TOA RFE and overlapping cloud fraction (R = 0.71), implying that overlapping cloud fraction can serve as a good predictor of springtime warming of dust aerosols at TOA over the northern Pacific Ocean on the daily timescale. There is about 1.11 W m^{-2} per unit τ_a increase in TOA RFE in response to 1% increase in overlapping cloud cover. The critical overlapping cloud fraction, for which RFE at TOA changes sign from negative to positive, is 0.20. Assuming absorbing aerosol (ω = 0.85 at 500 nm), Chand et al (2009) found a similar strong dependence on cloud cover fraction for the DRF of smoke aerosols over the partly cloudy boundary layer of the southeastern Atlantic Ocean, with a much slower critical cloud fraction (0.4). Differences in the definition of CF are likely to in part account for this discrepancy. Unlike underlying CF, overlapping CF only include the cloud features with overlying aerosol layers. On the basis of the Aqua data used herein, the mean overlapping cloud fraction over this region is 0.28, leading to a positive estimate for DRF ($0.62 Wm^{-2}$) as a whole. In addition, the value of DRF due to above-cloud dust aerosols is sensitive to uncertainties in ω of dust aerosols (Figure 7). An increase in ω (from 0.80 to 0.98)

leads to a decrease of 1.95 Wm^{-2} in DRF (from 1.62 to -0.33 Wm^{-2}). In other words, a change of ω by 0.02 roughly makes DRF to vary by almost 0.2 Wm^{-2} in each case.

5.4 Impact of underlying COD on all-sky TOA DRF due to ACDA

Previous studies suggested that the DRF variability of above-cloud aerosols is largely modulated by the cloud optical depth underneath (Zhang et al., 2014). Chand et al (2009) implied that aerosols overlying optically thick clouds would cause a much stronger warming effect, but they did not provide a quantitative relationship between cloud optical depth and DRF.

To demonstrate the impact of cloud optical depth on the springtime warming of dust aerosols, we analyze the relationship between the TOA RFE due to above-cloud dust aerosols and cloud optical depth under different ranges of overlapping cloud fraction (Figure 8). The positive trends indicate that dust aerosols over optically thick clouds would cause positive forcing. The reason is that dust aerosols above optically thick clouds tend to enhance the incident radiation reflected by clouds back to space and the absorption of dust aerosols of solar radiation, resulting in positive TOA forcing. On the other hand, dust aerosols above optically thin clouds cause negative TOA forcing, which is probably due to the cloud optical depth being so small to be able to be thought as clear skies. Over ocean, the scattering effect of dust aerosols in clear-sky is larger than the absorption of dust aerosols, leading to a negative DRF (i.e., cooling) at TOA. A closer examination reveals that the influence of cloud optical depth on the warming effect of dust aerosols depends on overlapping cloud fraction.

When overlapping cloud fraction falls below 0.2, dust aerosols over optically thick clouds even cause a negative DRF. Consistent with our previous discussions, if the overlapping cloud fraction is small, dust aerosols would intercept less solar radiation reflected by clouds. Therefore, even though dust aerosols are located above optically thick clouds, their DRF can still be negative. In contrast, in some nearly overcast cases when cloud fraction is above 0.8, the critical cloud optical depth doesn't even exist and dust forcing would be all warming effect. It can be easily understood that as the cloud fraction is large, dust aerosols would intercept large amount of solar radiation reflected by underlying clouds. Thus, even the cloud optical depth is small, the TOA DRF will still be positive.

When overlapping cloud fraction falls within the ranges from 0.2 to 0.8, the DRF would linearly increases with the cloud optical depth from negative to positive ($R \geq 0.69$), making it possible to define a critical cloud optical depth beyond which dust aerosols switch from exerting a net cooling to a net warming effect at top-of-atmosphere. Figure 8 (b), (c) and (d) show that the critical cloud optical depth decreases with the increases in overlapping cloud fraction. When overlapping cloud fraction ranges increases from 0.2 -0.4 to 0.6-0.8, the corresponding critical cloud optical depth reduces from 6.92 to 1.16.

6 Conclusions

In this study, the shortwave all-sky TOA DRF due to above-cloud dust aerosols over northern Pacific Ocean is quantitatively assessed using ten years (2007-2016) collocated CALIOP 5 km Aerosol and Cloud Layer products and MODIS L3 atmosphere product. The impact of overlapping cloud optical depth and cloud fraction on the warming effect of dust aerosols are also assessed by combining the satellite measurements and a radiation transfer model.

We find that the presence of underlying clouds boosts the absorption of solar radiation by dust aerosols. Thus dust aerosols have a significantly warming effect on the regional radiation budget. Geographically, the mean DRF due to above-cloud dust aerosols over the northern Pacific is about 0.62 Wm^{-2}. The RFE of dust aerosols, which is independent of AOD, has a linear relationship with the overlapping fraction. Starting from a clear-sky condition, a larger overlapping fraction between dust and clouds below will reduce the cooling effect of dust aerosols. As overlapping fraction beyond a critical value, the RFE due to above-cloud dust aerosols changes its sign from negative to positive. The impact of the cloud optical depth on the warming effect of dust aerosols is less effective than that of overlapping fraction, but it still modulates the magnitude of DRF, especially when overlapping fraction falls in the ranges of 0.2-0.8.

Theoretically, dust aerosols above optically thick clouds tend to enhance the incident radiation reflected by clouds back to space. Hence when cloud optical depth underneath increased, the absorption of dust aerosols of solar radiation will be enlarged accordingly. Similarly, if dust aerosols above optically thin clouds, the elevated dust aerosols would generally intercept more solar radiation, thus, they will absorb more solar radiation in the atmosphere and decrease the net

incoming radiation fluxes at TOA, causing a warming effect at TOA. We summarize our current understanding of the role of overlapping cloud properties on the warming effect of dust aerosols in the schematic diagram of Figure 9, which indicates the way how overlapping cloud properties impact the TOA radiative forcing caused by dust aerosols in the presence of clouds. As a bright surface, cloud can reflect large amount of solar radiation back to the dust aerosol layer and enhance aerosol absorption of solar radiation. The larger the overlapping cloud fraction and cloud optical depth, the more likely the multiple scattering and absorbing between aerosol and cloud layers will occur. During the processes of the multiple scattering and absorbing, more incident solar irradiance is absorbed by the absorbing aerosol layer in the atmosphere, resulting in less solar energy back to space and an increase in the TOA radiative forcing. Hence, the strength of the warming effect from absorbing aerosol is highly sensitive to the cloud optical depth and coverage of overlapping clouds. Based on the analyses above, we demonstrate that the accurate knowledge of the overlapping fraction and cloud optical depth are critical to estimate the shortwave DRF due to above-cloud dust aerosols. Our results stress the importance of cloud properties for determining the springtime warming of dust aerosols.

As an initial effort toward systematical understanding above-cloud dust aerosols, this paper only discusses the impact of cloud properties on the springtime warming effect of dust aerosols. Many other parameters, such as the vertical locations of aerosols relative to the clouds, could also affect the DRF due to above-cloud dust aerosols. In future, we will explore the potential influence of vertical locations of aerosols relative to the clouds on the springtime warming effect of dust aerosols.

Acknowledgments

This work was supported by the Natural Science Foundation of China (NSFC) under grant 41590874, the National Key Research and Development Program of the Ministry of Science and Technology (MOST) of China (2016YFA0602003), NSFC (Grants 91544217, 41405035 and 41471301), MOST under grant 2015DFA20870, the Postdoctoral Science Foundation of China (2016M601196), and Chinese Academy of Meteorological Sciences under grant 2017Z005. We are grateful to NASA for make us freely get access to the CALIOP and MODIS data used here.

Last, but not least, we would like to thank the editor and three anonymous reviewers for their constructive comments, which help significantly to improve the quality of this manuscript.

References

Abel, S. J., H. J. Highwood, J. M. Haywood, and M. A. Stringer (2005), The direct radiative effect of biomass burning aerosols over southern Africa, *Atmos. Chem. Phys.*, **5**(7), 1999–2018, doi:10.5194/acp-5-1999-2005.

Chand, D., R. Wood, T. L. Anderson, S. K. Satheesh, and R. J. Charlson (2009), Satellite-derived direct radiative effect of aerosols dependent on cloud cover, *Nat. Geosci.*, **2**, 181–184, doi:10.1038/NGEO437.

Chung, C. E., V. Ramanathan, D. Kim, and I. A. Podgorny (2005), Global anthropogenic aerosol direct forcing derived from satellite and ground-based observations, *J. Geophys. Res. Atmos*., **110**, D24207, doi: 10.1029/2005JD006356.

Clough, S. A., M. W. Shephard, E. J. Mlawer, J. S. Delamere, M. J. Iacono, K. Cady-Pereira, S. Boukabara, and P. D. Brown (2005), Atmospheric radiative transfer modeling: a summary of the AER codes, *J. Quant. Spectrosc. Radiat. Transfer*, **91**, 233–244.

Dai, T., G. Shi, and T. Nakajima (2015), Analysis and evaluation of the global aerosol optical properties simulated by an online aerosol-coupled non-hydrostatic icosahedral atmospheric model, *Adv. Atmos. Sci.*, **32**(6), 743-758, doi:10.1007/s00376-014-4098-z.

de Graaf, M., N. Bellouin, L. G. Tilstra, J. Haywood, and P. Stammes (2014), Aerosol direct radiative effect of smoke over clouds over the southeast Atlantic Ocean from 2006 to 2009, *Geophys. Res. Lett.*, **41**, 7723–7730, doi:10.1002/2014GL061103.

Devasthale, A., and M. A. Thomas (2011), A global survey of aerosol-liquid water cloud overlap based on four years of CALIPSO-CALIOP data, *Atmos. Chem. Phys.*, **11**, 1143–1154, doi:10.5194/acp-11-1143-2011.

Guo, J., M. Deng, S. S. Lee, et al. (2016a), Delaying precipitation and lightning by air pollution over the Pearl River Delta. Part I: Observational analyses, *J. Geophys. Res. Atmos.*, 121, 6472–6488, doi:10.1002/2015JD023257.

Guo, J., Liu, H., Wang, F., et al. (2016b), Three-dimensional structure of aerosol in China: A perspective from multi-satellite observations, *Atmos. Res.*, **178**, 580–589, doi:10.1016/j.atmosres.2016.05.010.

Guo J.P., T.N. Su, Z.Q. Li, Y.C. Miao, J. Li, H. Liu, H. Xu, M. Cribb, P.M. Zhai (2017a). Declining summertime local-scale precipitation over eastern China from 1970 to 2010 and its potential link to aerosols, *Geophys. Res. Lett.*, 44(11), 5700–5708, doi: 10.1002/2017GL073533.

Guo J.P., Lou M.Y., Miao Y.C., Wang Y., Zeng Z.L., Liu H., He J., Xu H., Wang F., Min M., and Zhai P.M. (2017b). Trans-Pacific transport of dust aerosol originated from East Asia: Insights gained from multiple observations and modeling, *Environ. Pol.* in press.

Hansen, J., M. Sato, and R. Ruedy (1997), Radiative forcing and climate response, *J. Geophys. Res. Atmos.*, **102**(D6), 6831–6864.

Herman, J. R., P. K. Bhartia, O. Torres, C. Hsu, C. Seftor, and E. Celarier (1997), Global distribution of UV-absorbing aerosols from Nimbus7/TOMS data, *J. Geophys. Res.*, **102**(D14), 16,911–16,922, doi:10.1029/96JD03680.

Holzer, M., I. G. Mckendry, and D. A. Jaffe (2003), Springtime trans-Pacific atmospheric transport from east Asia: A transit-time probability density function approach, *J. Geophys. Res. Atmos.*, **108**(22), 1771–1796. doi: 10.1029/2003JD003558.

Huang, K., G. Zhuang, J. Li, Q. Wang, Y. Sun, Y. Lin, and J. S. Fu (2010), Mixing of Asian dust with pollution aerosol and the transformation of aerosol components during the dust storm over China in spring 2007, *J. Geophys. Res. Atmos.*, **115**, D7, doi: 10.1029/2009JD013145.

IPCC 2007: Climate Change 2007. The Physical Science Basis. Contribution of Working Group I to the Fourth Assessment Report of the Inter-governmental Panel on Climate Change [Solomon, S., Qin, D., Manning, M., Marquis, M., Averyt, K. M. B., Tignor, M., Miller, H. L., and Chen, Z. (eds.)]. Cambridge, UK: Cambridge University Press.

Kahn, R. A., B. J. Gaitley, J. V. Martonchik, D. J. Diner, and K. A. Crean (2005), Multiangle Imaging Spectroradiometer (MISR) global aerosol optical depth validation based on 2 years of coincident Aerosol Robotic Network (AERONET) observations, *J. Geophys. Res. Atmos.*, **110**, D10S04, doi:10.1029/2004JD004706.

Keil, A., and J. M. Haywood (2003), Solar radiative forcing by biomass burning aerosol particles during SAFARI 2000: A case study based on measured aerosol and cloud properties, *J. Geophys. Res. Atmos.*, **108**, 8467, doi:10.1029/2002JD002315.

Kim, K. W., Z. He, and Y. J. Kim (2004), Physicochemical characteristics and radiative properties of Asian dust particles observed at Kwangju, Korea, during the 2001 ACE-Asia intensive observation period, *J. Geophys. Res.*, **109**, D19S02, doi:10.1029/2003JD003693.

Levelt, P. F., G. H. J. van den Oord, M. R. Dobber, et al. (2006), The Ozone Monitoring Instrument, *IEEE Trans. Geosci. Remote Sens.*, **44** (5), 1093 - 1101.

Levy, R. C., L. A. Remer, D. Tanre, S. Mattoo, and Y. J. Kaufman (2009), Algorithm for remote sensing of tropospheric aerosol over dark targets from MODIS: Collections 005 and 051: Revision 2, MODIS Algorithm Theoretical Basis Document for the MOD04_L2 Product.

Li Z., W.K.-M. Lau, V. Ramanathan, et al. (2016), Aerosol and Monsoon Climate Interactions over Asia, *Rev. Geophy.*, **54**(4), 866–929, doi: 10.1002/2015RG000500.

500 Liu, Z., M. Vaughan, D. Winker, C. Kittaka, B. Getzewich, R. Kuehn, A. Omar, K. Powell, C.
501 Trepte, and C. Hostetler (2009), The CALIPSO Lidar Cloud and Aerosol Discrimination:
502 Version 2 Algorithm and Initial Assessment of Performance, *J. Atmos. Ocean. Technol.*, **26**,
503 1198–1213, doi:10.1175/2009JTECHA1229.1.
504 Ma, C., S. Tohno, and M. Kasahara (2005), A case study of the size-resolved individual particles
505 collected at a ground-based site on the west coast of Japan during an Asian dust storm event,
506 *Atmos. Environ.*, **39**, 739–747, doi:10.1016/j.atmosenv.2004.09.073.
507 Meyer, K., S. Platnick, L. Oreopoulos, and D. Lee (2013), Estimating the direct radiative effect
508 of absorbing aerosols overlying marine boundary layer clouds in the southeast Atlantic
509 using MODIS and CALIOP, *J. Geophys. Res. Atmos.*, **118**, 4801–4815,
510 doi:10.1002/jgrd.50449, 2013.
511 Min, M., and Z. Zhang (2014), On the influence of cloud fraction diurnal cycle and sub-grid
512 cloud optical thickness variability on all-sky direct aerosol radiative forcing, *J. Quant.*
513 *Spectr. Radiat.*, **142**, 25–36, doi:10.1016/j.jqsrt.2014.03.014, 2014.
514 Murayama, T. N. et al. (2001), Ground-based network observation of Asian dust events of April
515 1998 in East Asia, *J. Geophys. Res. Atmos.*, **106**, 18345–60.
516 Mori, I., M. Nishikawa, T. Tanimura, and H. Quan (2003), Change in the size distribution and
517 chemical composition of kosa (Asian dust) aerosol during long-range transport, *Atmos.*
518 *Environ.*, **37**, 4253–4263, doi:10.1016/S1352-2310(03)00535-1.
519 Noh, Y. M. (2014), Single-scattering albedo profiling of mixed Asian dust plumes with
520 multiwavelength Raman lidar, *Atmos. Environ.*, **95**, 305–317, doi:
521 10.1016/j.atmosenv.2014.06.028.
522 Oikawa, E., T. Nakajima, T. Inoue, and D. Winker (2013), A study of the shortwave direct
523 aerosol forcing using ESSP/CALIPSO observation and GCM simulation, *J. Geophys. Res.*
524 *Atmos.*, **118**(9), 3687–3708.
525 Omar, A. H., D. M. Winker, M. A. Vaughan, Y. Hu, C. R. Trepte, R. A. Ferrare, K.-P. Lee, C. A.
526 Hostetler, C. Kittaka, and R. R. Rogers (2009), The CALIPSO automated aerosol
527 classification and lidar ratio selection algorithm, *J. Atmos. Ocean. Technol.*, **26**, 1994–2014,
528 doi:10.1175/2009JTECHA1231.1.
529 Podgorny, I. A., and V. Ramanathan (2001), A modeling study of the direct effect of aerosols
530 over the tropical Indian Ocean, *J. Geophys. Res.*, **106,** D20, 24,097**–**24,105.
531 Powell, K., C. A. Hostetler, Z. Liu, et al. (2009), CALIPSO lidar calibration algorithms. Part I:
532 Nighttime 532-nm parallel channel and 532-nm perpendicular channel, *J. Atmos. Oceanic*
533 *Technol.*, **26**(10), doi: 10.1175/2009JTECHA1242.1.

534 Platnick, S., M. D. King, S. A. Ackerman, W. P. Menzel, B. A. Baum, J. C. Riédi, and R. A.
535 Frey (2003), The MODIS Cloud Products: Algorithms and Examples From Terra, *IEEE*
536 *Trans. Geosci. Remote Sens.*, **41**(2), 459–473, doi: 10.1109/TGRS.2002.808301.
537 Remer, L., Y. Kaufman, D. Tanre, S. Mattoo, D. Chu, J. L. Martins, R.-R. Li, C. Ichoku, R. C.
538 Levy, and R. G. Kleidman (2005), The MODIS aerosol algorithm, products, and validation,
539 *J. Atmos. Sci.*, **62** (4), 947–973.
540 Salomonson, V. V., W. Barnes, P. W. Maymon, H. E. Montgomery, and H. Ostrow (1989),
541 MODIS: advanced facility instrument for studies of the Earth as a system, *IEEE Trans.*
542 *Geosci. Remote Sens.*, **27**, 145–153, doi: 10.1109/36.20292.
543 Schulz, M., C. Textor, S. Kinne, Y. Balkanski, S. Bauer, T. Berntsen, O. Boucher, F. Dentener,
544 S. Guibert, I. S. A. Isaksen, T. Iversen, D. Koch, A. Kirkevåg, X. Liu, V. Montanaro, G.
545 Myhre, J. E. Penner, G. Pitari, S. Reddy, Ø. Seland, P. Stier, and T. Takemura (2006),
546 Radiative forcing by aerosols as derived from the AeroCom present-day and preindustrial
547 simulations, *Atmos. Chem. Phys.*, **6**, 5225–5246, doi:10.5194/acp-6-5225-2006.
548 Shen, Z. B., and L. Wei (2000), Radiative effects of atmospheric dust aerosol in northwest China,
549 *Chin. J. Atmos. Sci.*, **24**(4), 541–548.
550 Sokolik, I. N., D. M. Winker, G. Bergametti, D. A. Gillette, G. Carmichael, Y. J. Kaufman, L.
551 Gomes, L. Schuetz, and J. E. Penner (2001), Introduction to special section: Outstanding
552 problems in quantifying the radiative impacts of mineral dust, *J. Geophys. Res. Atmos.*, **106**,
553 D16: 18015–18027.
554 Stephens, G. L., D. G. Vane, R. J. Boain, G. G. Mace, K. Sassen, Z. Wang, A. Illingworth, E.
555 O'Connor, W. B. Rossow, S. L. Durden, S. D. Miller, R. T. Austin, A. Benedetti, C.
556 Mitrescu, and the CloudSat Science Team (2002), The CloudSat mission and the A-Train:
557 A new dimension of space-based observation of clouds and precipitation, *Bull. Amer.*
558 *Meteor. Soc.*, **83**(12), 1771–1790.
559 Stier, P., Schutgens, N. A. J., Bellouin, N., Bian, H., Boucher, O., Chin, M., Ghan, S., Huneeus,
560 N., Kinne, S., Lin, G., Ma, X., Myhre, G., Penner, J. E., Randles, C. A., Samset, B., Schulz,
561 M., Takemura, T.,Yu, F.,Yu, H., and Zhou, C (2013), Host model uncertainties in aerosol
562 radiative forcing estimates: results from the AeroCom Prescribed intercomparison study,
563 *Atmos. Chem. Phys.*, **13**, 3245–3270, doi:10.5194/acp-13-3245-2013.
564 Sun, J., M. Y. Zhang, and T. S. Liu (2001), Spatial and temporal characteristics of dust storms in
565 China and its surrounding regions, 1960–1999: Relations to source area and climate, *J.*
566 *Geophys. Res.*, **106**, 10,325–10,333, doi:10.1029/2000JD900665.
567 Takemura, T., T. Nakajima, O. Dubovik, B. N. Holben, and S. Kinne (2002), Single scattering
568 albedo and radiative forcing of various aerosolspecies with a global three-dimensional
569 model, *J. Clim.*, **15**, 333–352.

570 Textor, C., M. Schulz, S.Guibert, S., et al. (2006), Analysis and quantification of the diversities
571 of aerosol life cycles within AeroCom, *Atmos. Chem. Phys.*, **6**, 1777–1813.
572 Torres, O., A. Tanskanen, B. Veihelmann, C. Ahn, R. Braak, P. K. Bhartia, P. Veefkind, and P.
573 Levelt (2007), Aerosols and surface UV productsfrom Ozone Monitoring Instrument
574 observations: An overview, *J. Geophys. Res.*, **112**, D24S47, doi:10.1029/2007JD008809.
575 Vaughan, M., S. Young, D. Winker, K. Powell, A. Omar, Z. Liu, Y. Hu, and C. Hostetler (2004),
576 Fully automated analysis of space-based lidar data: An overview of the CALIPSO retrieval
577 algorithms and data products, Proc. SPIE, **5575**, 16–30.
578 Vaughan, M. A., K. A. Powell, R. E. Kuehn, et al. (2009), Fully automated detection of cloud
579 and aerosol layers in the CALIPSO lidar measurements, *J. Atmos. Oceanic Technol.*, **26**,
580 2034–2050.
581 Wang, H., X. Zhang, S. Gong, Y. Chen, G. Shi, and W. Li (2010), Radiative feedback of dust
582 aerosols on the East Asian dust storms, *J. Geophys. Res. Atmos.*, **115**, D23214, doi:
583 10.1029/2009JD013430.
584 Wang, Y., A. Khalizov, M. Levy, and R. Zhang (2013), New Directions: Light Absorbing
585 Aerosols and Their Atmospheric Impacts, *Atmos. Environ.*, **81**, 713–715.
586 Wang, Y., M. Wang, R. Zhang, S. J. Ghan, Y. Lin, J. Hu, B. Pan, M. Levy, J. Jiang, and M. J.
587 Molina (2014), Assessing the effects of anthropogenic aerosols on Pacific storm track using
588 a multi-scale global climate model, Proc. Natl Acad. Sci. USA, 111(19), 6894–6899.
589 Wang, Y., J. Jiang, and H. Su (2015), Atmospheric responses to the redistribution of
590 anthropogenic aerosols, *J. Geophys. Res. Atmos.*, **120**(18), 9625–9641.
591 Winker, D. M., W. Hunt, and M. McGill (2007), Initial performance assessment of CALIOP,
592 *Geophys. Res. Lett.*, **34**, L19803, doi:10.1029/2007GL030135.
593 Winker, D. M., M. A. Vaughan, A. Omar, Y. Hu, K. A. Powell, Z. Liu, W. H. Hunt, and S. A.
594 Young (2009), Overview of the CALIPSO mission and CALIOP data processing algorithms,
595 *J. Atmos. Ocean. Tech.*, **26**, 2310–2323.
596 Winker, D. M., J. L. Tackett, B. J. Getzewich, Z. Liu, M. A. Vaughan, and R. R. Rogers (2013),
597 The global 3-D distribution of tropospheric aerosols as characterized by CALIOP, *Atmos.
598 Chem. Phys.*, **13**, 3345–3361, doi:10.5194/acp-13-3345-2013.
599 Wiscombe, W. (1980), Improved Mie scattering algorithms, *Appl. Opt*, **19**, 1505–1509.
600 Xu, H., J. Guo, X. Ceamanos, J. L. Roujean, M. Min, and D. Carrer (2016), On the influence of
601 the diurnal variations of aerosol content to estimate direct aerosol radiative forcing using
602 MODIS data, *Atmos. Environ.*, **141**, 186–196.
646 Zhang, J., S. M. Liu, X. Lu, and W. W. Huang (1993), Characterizing Asian wind-dust transport
647 to the northwest Pacific Ocean: Direct measurements of dust flux for two years, *Tellus, Ser.
648 B*, **45**, 335–345.

649 Zhang, Z., K. Meyer, S. Platnick, L. Oreopoulos, D. Lee, and H. Yu (2014), A novel method for
650 estimating shortwave direct radiative effect of above-cloud aerosols using CALIOP and
651 MODIS data, *Atmos. Meas. Tech.*, **7**, 1777–1789, doi:10.5194/amt-7-1777-2014.
652 Zhang, Z., K. Meyer, H. Yu, S. Platnick, P. Colarco, Z. Liu, and L. Oreopoulos (2016),
653 Shortwave direct radiative effects of above-cloud aerosols over global oceans derived from 8
654 years of CALIOP and MODIS observations, Atmos. Chem. Phys., 16, 2877–2900,
655 doi:10.5194/acp-16-2877-2016.

Tables

Table 1. Quality control metrics used for screening the CALIOP aerosol layer product.

CALIOP product parameter	Criterion
CAD	-20 to -100
Extinction_QC_532	0 or 1
Feature_optical_depth_uncertainty_532	<99.9

Figures

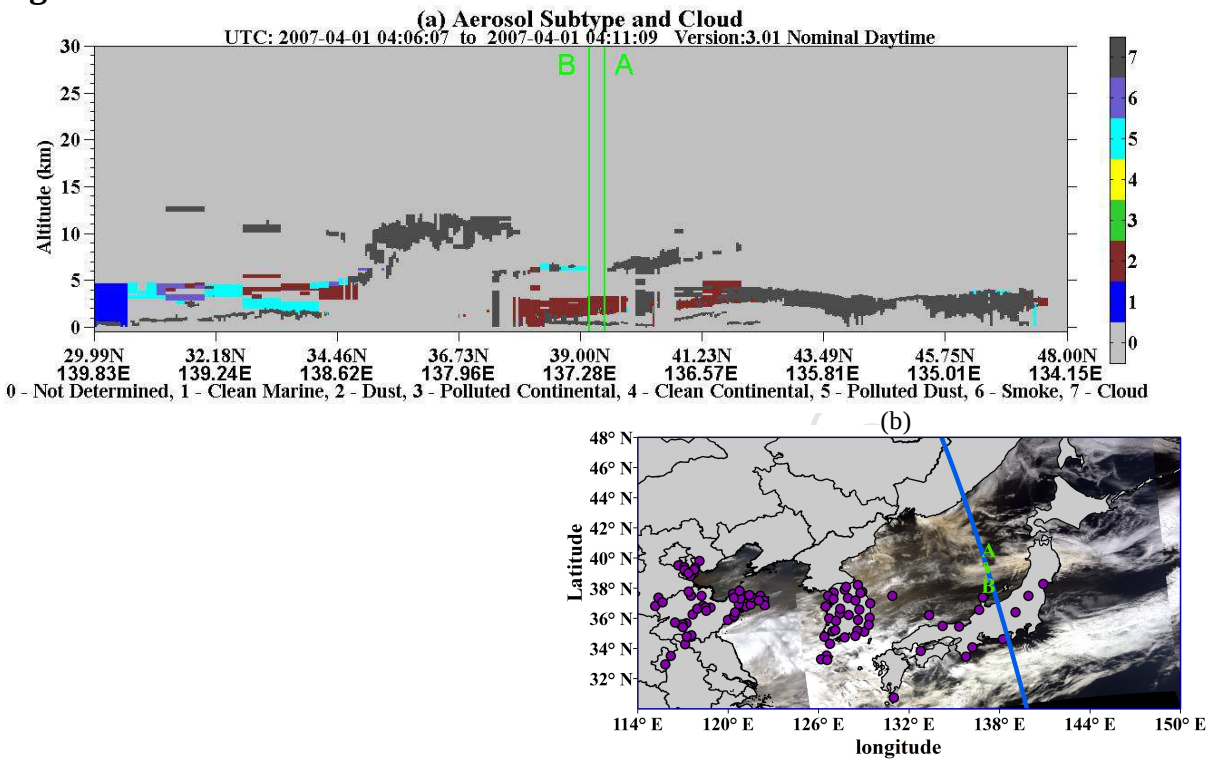

Figure 1. A composite map showing the typical episode of above-cloud dust aerosol occurring on 1st April 2007. (a) Curtain plot of aerosol subtypes and cloud from CALIOP/CALIPSO along the segment of a CALIPSO daytime ground track (in ascending mode) shown in (b). Dust aerosols and clouds are denoted with red and dark grey color, respectively. (b) MODIS/AQUA RGB composite (created using visible bands 1/4/3), overlaid are dust phenomena (marked in purple points) simultaneously observed at the surface weather stations. The green segment marked with A-B in both panel (a) and (b) refers to one typical example representing dust aerosol over cloud.

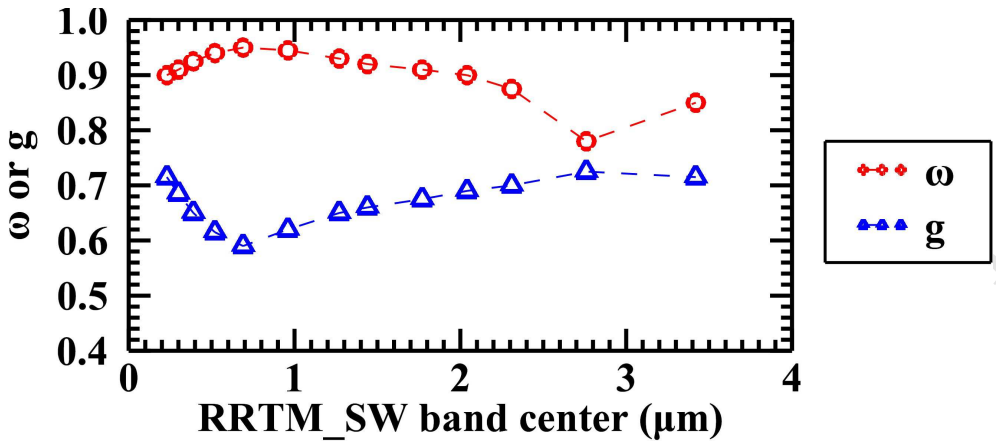

Figure 2. Single scattering albedo (ω) and phase function (g) of dust aerosol for each band of RRTM_SW (Omar et al., 2009).

(a)

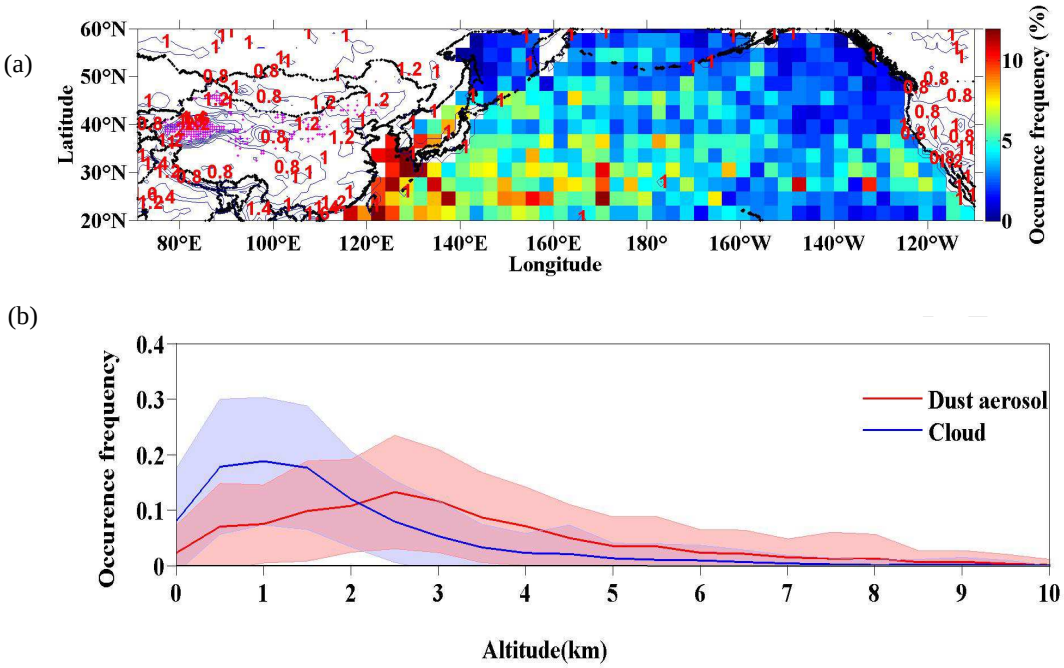

Figure 3. (a) Spatial distribution of occurrence frequency (OF) of ACDA, and (b) OF vertical profiles of dust aerosols and clouds over the northern Pacific Ocean in spring as calculated from 10-year (2007-2016) daytime CALIOP observations. Note that in (a) the magenta-shaded area indicates the major source region of dust in both western and northern China, and the blue contour lines (intervals of 0.2) indicate the OMI absorbing aerosol index (AI). In (b) the red (blue) shadow area represents one standard deviation of the mean OF of dust aerosol (cloud).

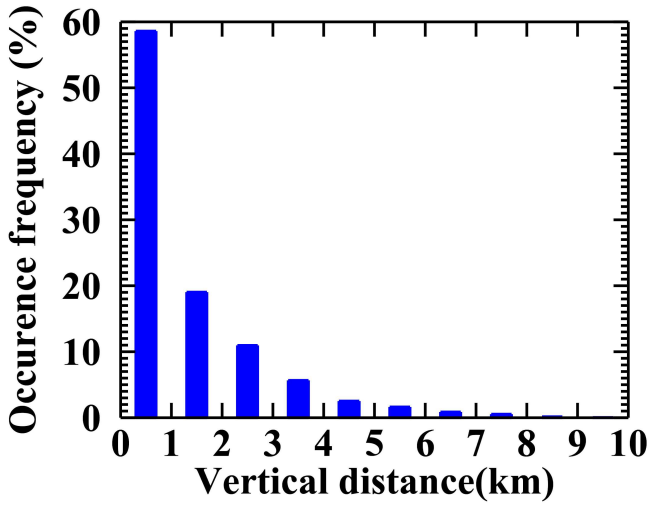

Figure 4. Histogram of the distance from the bottom of dust aerosol layer to underlying cloud layer top (at intervals of 1km) for all the overlapping cases in springs of the period 2007-2016.

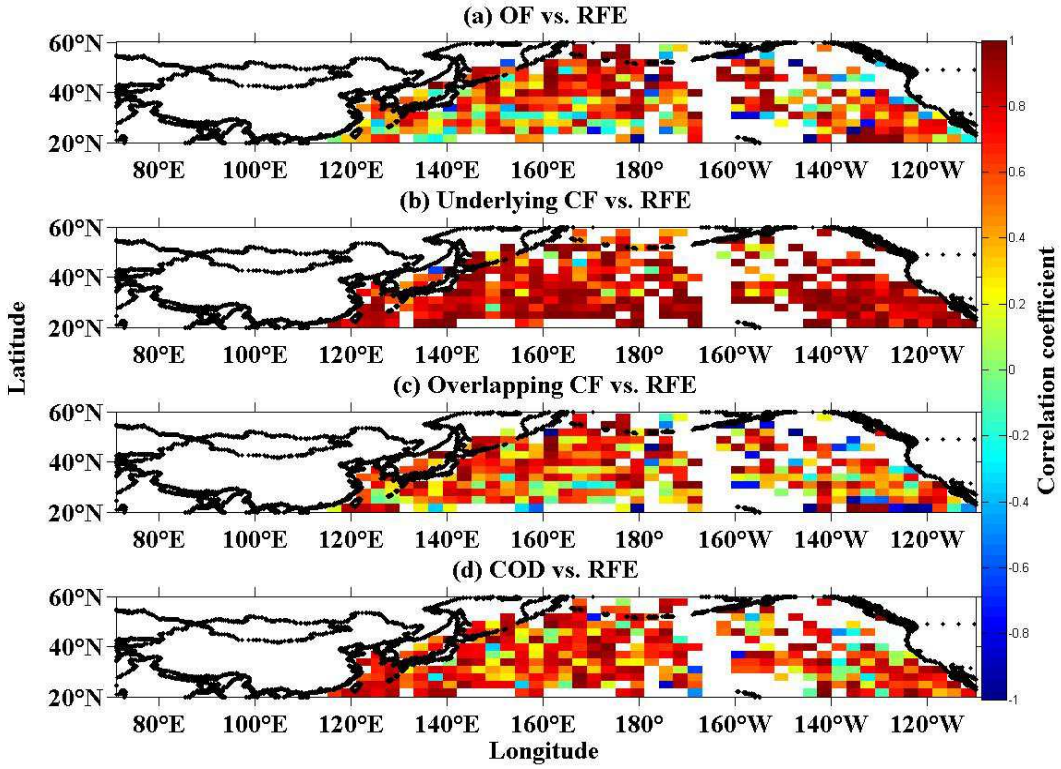

Figure 5. Spatial distributions of the correlation coefficients (R) between TOA RFE and occurrence frequency of ACDA (a), and underlying CF (b), overlapping CF of ACDA (c), and COD (d), respectively, in springs for the period 2007 to 2016.

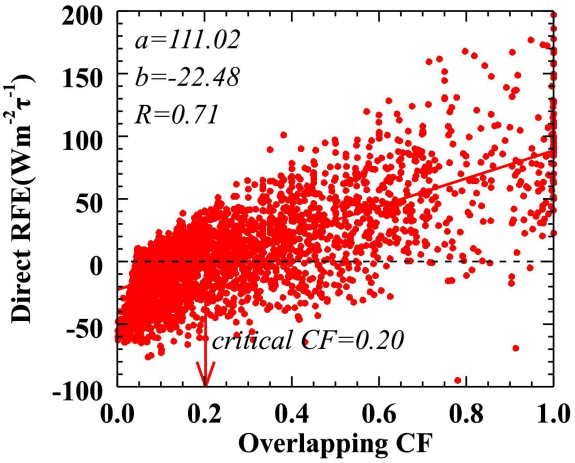

Figure 6. Scatter plot of TOA direct radiative forcing efficiency (RFE) due to ACDA as a function of overlapping cloud fraction (CF) in springs for the period 2007 to 2016. Critical CF is defined as the overlapping cloud fraction at which the sign of TOA RFE changes. The texts on top left corner of the figure show the slopes (a), intercepts (b), and correlation coefficient (R) of the regression lines. The RRTM_SW model is run using spectrally dependent single scattering albedo (ω) and phase function (g) of dust aerosols shown in Figure 2.

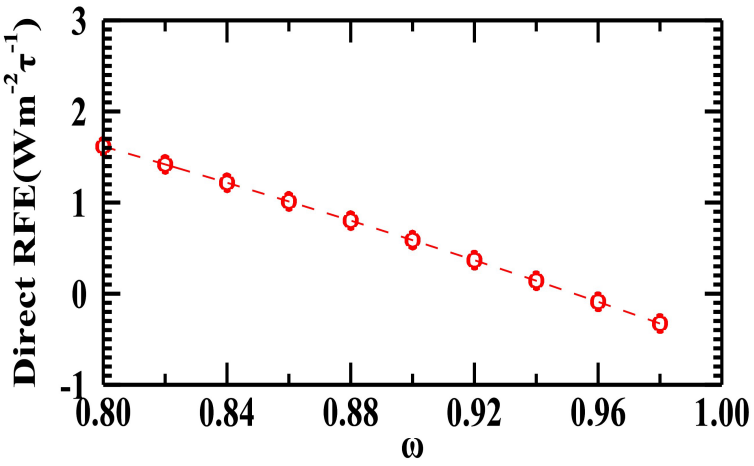

Figure 7. Scatter plot of TOA direct radiative forcing efficiency (RFE) due to ACDA with respect to its corresponding single scattering albedo (ω).

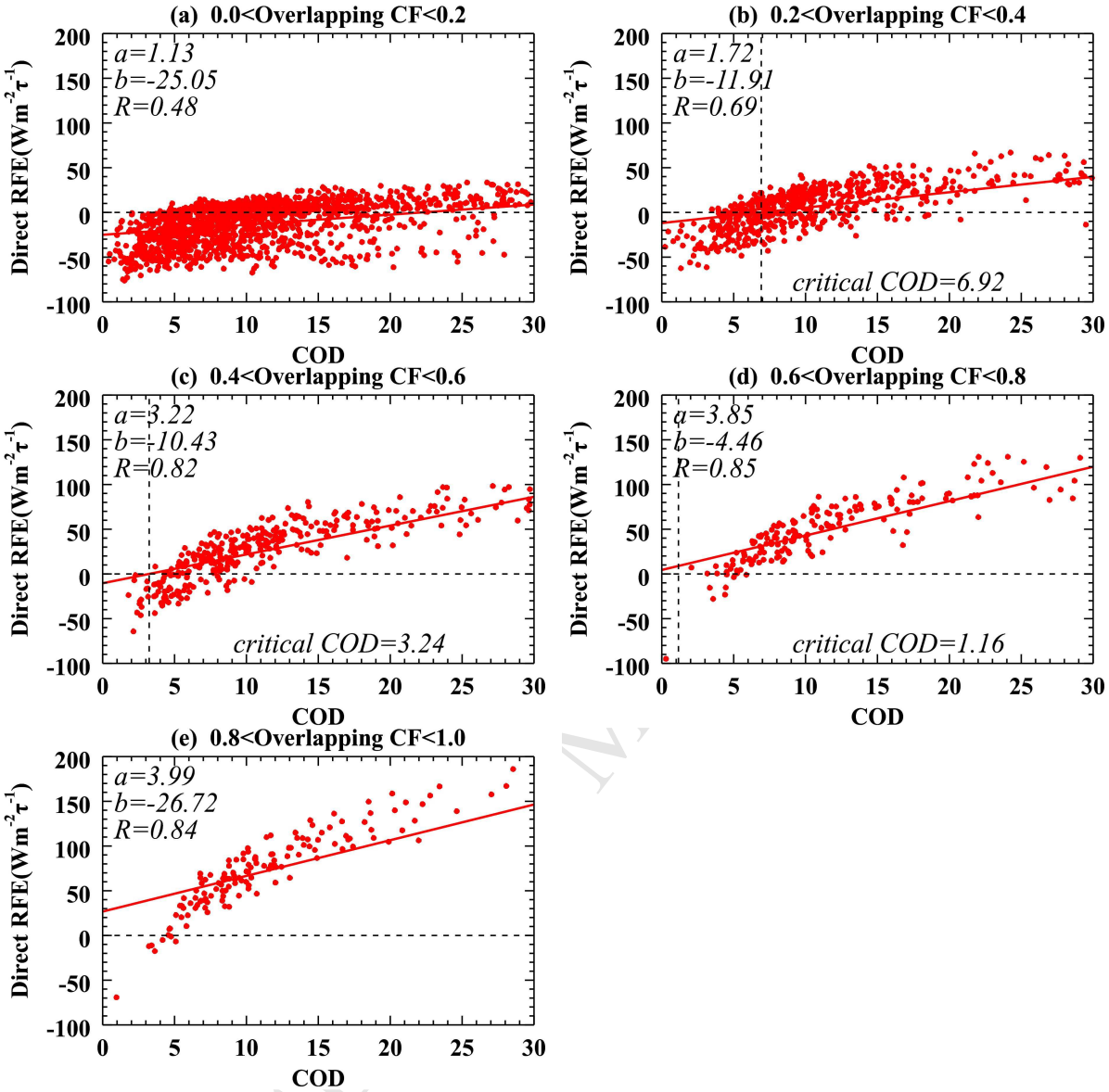

Figure 8. Correlation between the TOA direct RFE due to ACDA and overlapping cloud optical depth (COD) under the condition of overlapping CF falling in the range [0.0,0.2] (a), [0.2,0.4] (b), [0.4,0.6] (c), [0.6,0.8] (d) and [0.8,1.0] (e) in springs for the period 2007 to 2016. The critical COD in (b), (c) and (d) is the cloud optical depth at which the sign of TOA direct RFE changes under the condition of overlapping CF falling in the range [0.2,0.4], [0.4,0.6] and [0.6,0.8], respectively. The RRTM_SW model is run using spectrally dependent single scattering albedo (ω) and phase function (g) of dust aerosols shown in Figure 2.

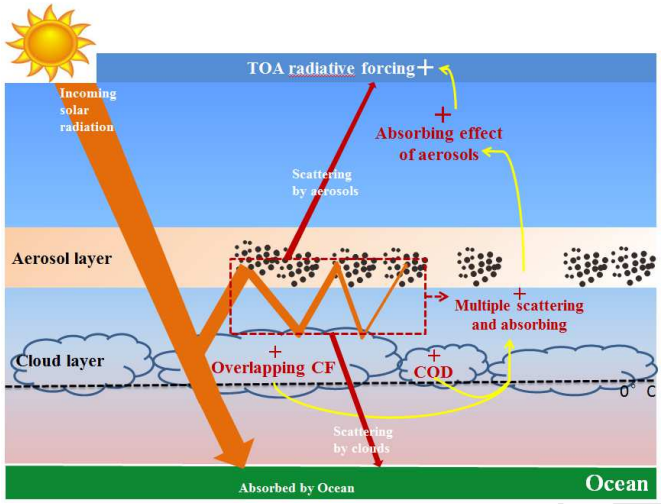

Figure 9. Schematic diagram of the factors affecting TOA radiative forcing of ACDA, which is initiated by increased cloud optical depth, overlapping cloud fraction, and multiple scattering and absorbing.

- In spring, frequency of above-cloud dust aerosols over northern Pacific Ocean is high up to 0.12.
- The springtime warming effect of above-cloud dust aerosols increases with overlapping cloud fraction and cloud optical depth.
- The critical cloud optical depth for dust effect depends on the concurrent overlapping cloud fraction.